Proc. 4th Int'l Conf. on Statistical Climatology, Rotorua, New Zealand, March 1989,

Marine stratocumulus spatial structure

Robert F. Cahalan[1], M. Nestler[2], W. Ridgway[3], W.J. Wiscombe[1] T. Bell[1]
[1]Laboratory for Atmospheres, Goddard Space Flight Center, Greenbelt; [2]Science Applications Research, Lanham; [3]Applied Research Corporation, Landover, MD, USA

Introduction

Many theoretical studies have shown the sensitivity of cloud radiative properties to their spatial structure, ranging from the seminal work of McKee and Cox (1974) and Stephens (1976) to more recent work by Harshvardan and Weinman (1982), Welch and Wielicki (1985), and others. As Harshvardan and Randall (1985) have pointed out, current general circulation models, because of their reliance on plane-parallel assumptions, are in the embarrassing situation of having to use unrealistically small liquid water amounts to produce realistic albedos. Stephens (1985) has emphasized that the mean albedo is not a function of mean liquid water alone, but depends upon its spatial distribution. Lovejoy (1982) suggested that cloud spatial distributions may be modelled as self-similar fractals, and has more recently generalized to multifractals (Schertzer and Lovejoy, 1988). Rhys and Waldvogel (1986) and others have shown that cloud fractal dimensions undergo abrupt changes at certain scales, and Cahalan and Joseph (1989) found that these characteristic scales depend upon cloud type.

Marine stratocumulus are perhaps closest to plane-parallel, being largely confined between the lifting condensation level and the strong subtropical inversion. In a recent study of marine stratocumulus, using data from FIRE (summarized by Albrecht et al.), Cahalan and Snyder (1989, hereafter CS) found a change in the stratocumulus wavenumber spectrum from a -5/3 power to a -3 power at a scale determined by the cloud thickness, a few hundred meters. This is consistent with two- dimensional homogeneous turbulence (Kraichnan, 1967), in which energy injected at a particular scale (e.g. the cloud thickness) cascades to lower wavenumbers with a -5/3 power law, while the enstropy cascades to higher wavenumbers with a -3. Observations by commercial aircraft (Gage and Nastrom, 1986) show a -3 at low wavenumbers, presumably from baroclinic forcing at a few thousand km, changing at a few hundred kilometers to a -5/3, which we suggest is associated with convective forcing at the cloud thickness scale. In the following we briefly summarize the stratocumulus observations, then present a simple model for the observed structure.

Observed Stratocumulus Structure

Much of our knowledge of stratocumulus horizontal structure is based upon observations of cloud reflectivity (see e.g. Cahalan and Joseph, 1989; for vertical structure see Boers and Betts, 1988). A more basic question is how the cloud liquid water is distributed, since the reflectivity can be computed from the distribution of liquid water, traditionally by specifying microscopic properties like drop sizes, and macroscopic properties like optical depth, etc.. The radiation field provides a kind of low-pass spatial filter, so that there may be small-scale variations of liquid water to which the LANDSAT data are completely insensitive (Cahalan, 1988b). [At the same time, the mesoscale structure of stratocumulus liquid water, which leads to the power-law wavenumber spectrum described below, is to some extent mirrored in the reflectivity data, which follows the same power-law (CS).] These liquid water variations are not included in our usual plane-parallel computations, and will be an important input to more realistic radiative transfer models.

Vertically integrated liquid water was measured at 1 minute intervals over a three-week period during FIRE (see CS for details). The histogram of this data is shown in figure 1a on a log-linear scale, with a lognormal fit plotted for comparison. The lognormal roughly follows the data, while differing in detail. The "shoulders" seen to each side of the observed central peak are a reminder that

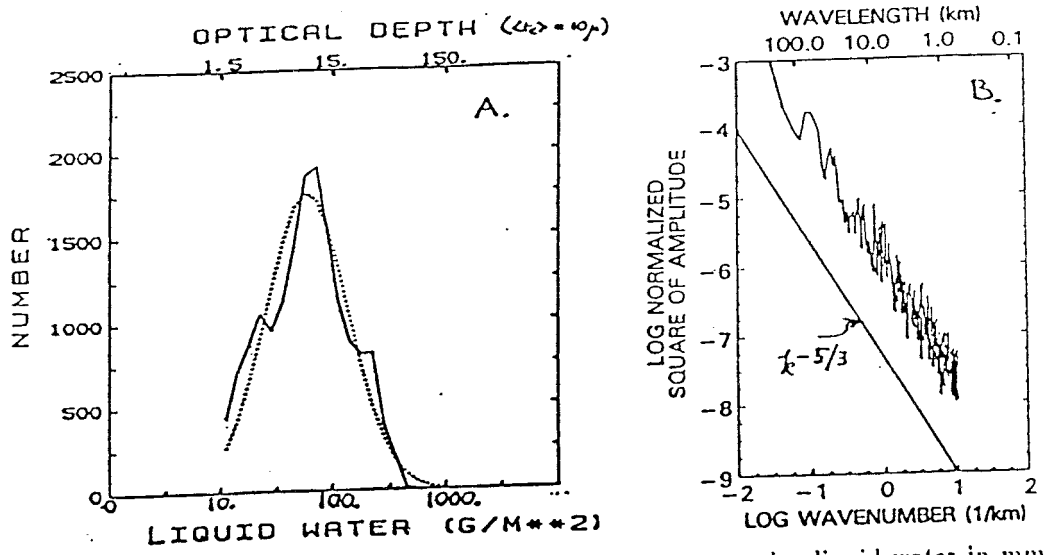

Figure 1: (a) Probability distribution of vertically integrated stratocumulus liquid water in mm plotted on a log-linear scale, along with a lognormal fit. The equivalent optical depth scale shown at the top assumes a 10 micron effective radius. (b) Wavenumber spectrum of integrated liquid water computed from time series assuming 5 m/s frozen turbulence.(CS)

individual days often show a bimodal distribution. The liquid water wavenumber spectrum (fig.1b) was estimated from the frequency spectra computed from several one-day time series of one-minute averages of total vertically integrated liquid water measured at San Nicolas Island during FIRE. Results were translated from frequency to wavenumber assuming frozen turbulence with a 5 m/s mean advection. The least-squares fit from about 400 km down to about 400 m gives $S(k) \sim k^{-5/3}$ (see Cahalan and Snider, 1989). By contrast, fair weather cumulus show a much flatter spectrum over the same scales (CS).

This is the classic Kolmogorov result for the wavenumber spectrum of any component of the velocity field, and is also the spectrum expected for a "passive scalar", i.e. a scalar field whose variations in space and time are due only to advection. This suggests that the total integrated liquid water in stratocumulus clouds fluctuates with the vertical velocity, being large in updrafts and small in downdrafts. This kind of behavior has been observed in fine-resolution numerical simulations (MacVean and Nicholls, 1988), though they do not reproduce the highly irregular fractal structure described above. Correlations of vertical velocity and liquid water will be of much interest as more of the FIRE data is analyzed.

Fractal Stratocumulus Streets

In this section we first describe a technique for analyzing wavenumber spectra which is especially convenient for cascade models. We then consider two simple multiplicative cascade models which give spatial distributions of liquid water which are fractal in one horizontal dimension, and uniform in the other horizontal direction and in the vertical. Both models give lognormal-like probability densities of optical depth. However, the range of optical depths in the first model is unbounded as the resolution increases, while the second model has both an upper and lower bound. The first model also produces a wavenumber spectrum flatter than k^{-1}, while the second model may be tuned to reproduce the observed $k^{-5/3}$.

Spectral analysis preliminaries

Consider a stochastic function of position $f(x)$, which is homogeneous over some domain L_0, and let $f'(x)$ be the deviation from the mean, so that $\langle f'(x) \rangle = 0$, where the angular brackets indicate an ensemble average. The associated lag covariance function is then given by

$$c(x) = \langle f'(x_0)\, f'(x_0 + x) \rangle. \tag{1}$$

The power spectrum may be computed from the covariance by Fourier transform, so that

$$S(k) = \int_{-\infty}^{\infty} dx\, e^{-ikx}\, c(x). \tag{2}$$

A simple approach to analyzing the spectrum, which turns out to be particularly convenient for multiplicative cascade models, is Lorenz' "poor man's spectral analysis" (Lorenz, E. N., 1979). We consider averages of $f(x)$ over successively smaller subdivisions of the domain:

$$\overline{f}_n(x) = \frac{1}{L_n} \int_0^{L_n} dx\, f(x), \tag{3}$$

where each interval, L_n, is half as big as the previous:

$$L_n = \frac{L_0}{2^n}. \tag{4}$$

The variance of $\overline{f}_n$ is then

$$\begin{aligned} V_n &= \langle (\overline{f}_n)^2 \rangle \\ &= \frac{1}{L_n^2} \int_0^{L_n} dx_1 \int_0^{L_n} dx_2\, \langle f(x_1)\, f(x_2) \rangle \\ &= \frac{1}{L_n^2} \int_0^{L_n} dx_1 \int_0^{L_n} dx_2\, c(x_1 - x_2) + \langle f \rangle^2 \\ &= \frac{1}{L_n^2} \int_0^{L_n} dx_1 \int_0^{L_n} dx_2 \int_{-\infty}^{\infty} \frac{dk}{2\pi}\, e^{ik(x_1 - x_2)}\, S(k) + \langle f \rangle^2 \\ &= \int_{-\infty}^{\infty} \frac{dk}{2\pi}\, |\mathcal{F}(kL_n)|^2\, S(k) + \langle f \rangle^2, \end{aligned} \tag{5}$$

where

$$\mathcal{F}(kL_n) = \frac{1}{L_n} \int_0^{L_n} dx\, e^{ikx} = \frac{e^{ikL_n} - 1}{ikL_n}, \tag{6}$$

so that

$$|\mathcal{F}(z)|^2 = \frac{\sin^2(z/2)}{(z/2)^2} \tag{7}$$

To remove the mean in (5), we consider the **variance increment** defined as

$$\Delta V_n \stackrel{\text{def}}{=} V_n - V_{n-1}, \tag{8}$$

which gives the variance on scales L_n about the means over twice that scale. Using (5), (8) becomes

$$\Delta V_n = \int_{-\infty}^{\infty} \frac{dk}{2\pi}\, S(k)\, \mathcal{D}(kL_n), \tag{9}$$

with

$$\mathcal{D}(z) \stackrel{\text{def}}{=} |\mathcal{F}(z)|^2 - |\mathcal{F}(2z)|^2 = \left[\frac{\sin^2(z/2)}{z/2}\right]^2. \tag{10}$$

According to (9) ΔV_n is simply a filtered version of the spectrum $S(k)$, with the band-pass filter function $\mathcal{D}(kL_n)$ isolating power in the wavenumber interval centered on

$$k_n \stackrel{\text{def}}{=} \frac{\pi}{L_n}. \tag{11}$$

Inserting into (9) a power-law wavenumber spectrum,

$$S(k) \sim k^{-\alpha}, -1 < \alpha < 2, \tag{12}$$

the effect of the filter on the spectrum gives $k_n^{-\alpha}$, and an additional factor of k_n comes from the dk, so that

$$\Delta V_n \sim k_n^{1-\alpha} \sim L_n^{\alpha-1} \sim 2^{n(1-\alpha)}. \tag{13}$$

In other words, if we observe a variance increment as in (13), then the spectrum must have the power-law given by (12). Taking the natural log of both sides of (13), we find that the spectral exponent α may be determined by

$$\alpha = 1 - \frac{\ln(\Delta V_n)}{n \ln 2} \tag{14}$$

Simple cascade models

We consider a stratocumulus cloud confined between the lifting condensation level and the inversion height, and initially having a uniform distribution of liquid water with optical depth given by

$$\tau_0 = 10. \tag{15}$$

We consider an infinitely long slab of horizontal width L_0, and divide it into two slabs of width $L_0/2$. A fraction of the liquid water is transferred from one half to the other, with the direction chosen at random. The optical depth in one half is then increased by some fraction, say f_1 (due to increased density — thickness is assumed unchanged), and the other half is correspondingly optically thinner. This may be written

$$\tau_1^{(\pm)} = (1 \pm f_1)\tau_0. \tag{16}$$

where the superscript on the left side of (16) indicates whether the brighter or darker half is being considered.

To continue the process, each half is itself divided in half, and a fraction of liquid water, f_2, is transferred, again in a random direction, so that

$$\tau_2^{(\pm)} = (1 \pm f_2)\tau_1. \tag{17}$$

After iterating for $n+1$ steps, there are 2^{n+1} segments, each with an optical depth of the form

$$\tau_{n+1}^{(\pm)} = \prod_{k=1}^{n}(1 \pm f_k)\tau_0. \tag{18}$$

Any of the possible combinations of signs in (18) may be found somewhere among the 2^{n+1} segments. An upper bound on the optical depth of the optically thickest segment may be found from

$$\prod_{k=1}^{n}(1 + f_k) < \prod_{k=1}^{n} \exp(f_k) = \exp(\sum_{k=1}^{n} f_k) \tag{19}$$

The fractions f_n are assumed to be stictly between 0 and 1, and we consider two models:

$$f_n = f, \text{ (singular model)} \tag{20}$$

where f is constant, and

$$f_n = fc^n. \text{ (bounded model)} \tag{21}$$

where f and c are both constants between 0 and 1. The upper bound given by (19) diverges for the singular model, and it can be shown in this case that the liquid water becomes concentrated on a fractal set of singularities as $n \to \infty$. The upper bound for the bounded model is $\exp(fc/(1-c))\tau_0$ and provides a good estimate of τ_{max}.

From the variance increment defined in equation (8) we may compute the spectral exponent of both the singular model and the bounded model using (14). The computation is aided by the fact that the optical depth averaged over L_n is a constant independent of n, since liquid water is being conserved. Thus we may write

$$\begin{aligned} V_n &= \langle [\prod_{k=1}^{n} (1 \pm f_k)\tau_0]^2 \rangle \\ &= \prod_{k=1}^{n} \langle (1 \pm f_k)^2 \rangle \langle \tau_0^2 \rangle. \end{aligned} \tag{22}$$

While the optical depth is different for each segment in a given realization, the statistics are the same for all segments. If we let

$$\mu_k \stackrel{\text{def}}{=} \langle (1 \pm f_k)^2 \rangle, \tag{23}$$

then (22) may be written

$$V_n = [\prod_{k=1}^{n} \mu_k] \langle \tau_0^2 \rangle. \tag{24}$$

so that the variance increment becomes

$$\Delta V_n = [\prod_{k=1}^{n-1} \mu_k](\mu_n - 1)\langle \tau_0^2 \rangle. \tag{25}$$

For each of the models we obtain

$$\mu_k = 1 + f^2, \text{ (singular model)} \tag{26}$$

and

$$\mu_k = 1 + f^2 c^{2k}. \text{ (bounded model)} \tag{27}$$

so that the variance increment in (25) behaves for large n as

$$\Delta V_n \sim (1 + f^2)^n, \text{ (singular model)} \tag{28}$$

and

$$\Delta V_n = \left[\prod_{k=1}^{n-1} (1 + f^2 c^{2k})\right] f^2 c^{2n} \langle \tau_0^2 \rangle. \text{ (bounded model)} \tag{29}$$

Finally, using (14) we obtain

$$\alpha = 1 - \frac{\ln(1 + f^2)}{\ln 2}, \text{ (singular model)} \tag{30}$$

and

$$\alpha = 1 - 2\frac{\ln c}{\ln 2}. \text{ (bounded model)} \tag{31}$$

where we used the fact that the factor in square brackets in (29) becomes independent of n for large n. Note that as $f \to 1$ the exponent of the singular model goes to zero, giving a flat (white noise)

spectrum, while as $f \to 0$ the spectrum steepens to k^{-1}. No value of f allows the singular model to fit the observed $\alpha = 5/3$ spectrum shown in figure 1b. The exponent of the bounded model is independent of f, and if we choose $c = 2^{-1/3}$ we obtain $\alpha = 5/3$. The probability density is quite sensitive to the value of c, and often has considerable structure. However, when $c = 2^{-1/3}$ it is close to lognormal, and qualitatively agrees with figure 1a.

Conclusions

The simple 2-parameter model presented here gives a reasonable fit to two important properties of vertically integrated stratocumulus liquid water : the lognormal-like probability density, and the power-law wavenumber spectrum. The model is being used to determine the radiative properties of fractal clouds, and investigate the limits of plane-parallel theory. Each cascade step redistributes liquid water in an initially plane-parallel cloud while cloud height and mean optical depth are held fixed at each step. Redistribution invariably decreases the mean albedo from the plane parallel case, since the albedo of optically thick regions saturates as optical depth is increased. The albedo of each homogeneous region may be computed from the thickness of each region independently only when the horizontal optical depth is large compared to the photon mean free path. The albedo of a region comparable in horizontal optical depth to the photon mean free path depends upon radiation from the sides. The mean albedo is insensitive to variations in optical depth on horizontal scales much smaller than the photon mean free path. Further development of these concepts will be closely tied to realistic simulations of the turbulent structure of boundary-layer clouds observed during FIRE.

References

Albrecht, B.A., D.A. Randall, and S. Nicholls, 1988: Observations of marine stratocumulus clouds during FIRE, *Bull. Amer. Meteor. Soc., 69, 618-626.*

Boers, R., and A.K. Betts, 1988: Saturation point structure of marine stratocumulus clouds, *J. Atmos. Sci., 45, 1156-1175.*

Cahalan, R.F. 1988a: LANDSAT observations of fractal cloud structure, in *Scaling, Fractals and Nonlinear Variability in Geophysics, D. Schertzer and S. Lovejoy, ed., Kluwer, in press.*

Cahalan, R.F. 1988b: Overview of fractal clouds, in *Advances in Remote Sensing Retrieval Methods. A. Deepak Publishing, in press.*

Cahalan, R.F., and J.H. Joseph, 1989: Fractal statistics of cloud fields, *Mon. Wea. Rev., 117, 257-268.*

Cahalan, R.F., and J.B. Snider, 1989: Marine stratocumulus structure during FIRE, submitted to *Remote Sensing of the Environment.*

Gage, K.S. and G.D. Nastrom, 1986: Theoretical interpretation of atmospheric wavenumber spectra of wind and temperature observed by commercial aircraft during GASP, *J. Atmos. Sci., 43, 729-740.*

Harshvardhan and D.A. Randall, 1985: Comments on "The parameterization of radiation for numerical weather prediction and climate models", *Mon. Wea. Rev., 113, 1832-1833.*

Harshvardan and J.A. Weinman, 1982: Infrared radiative transfer through a regular array of cuboidal clouds, *J. Atmos. Sci., 39, 431-439.*

Kraichnan, R.H., 1967: Inertial ranges in two-dimensional turbulence, *Phys. Fluids, 10, 1417-1423.*

Lorenz, E.N., 1979: Forced and free variations of weather and climate, *J. Atmos. Sci., 36, 1367-1376.*

Lovejoy, S., 1982: Area-perimeter relation for rain and cloud areas, *Science, 216, 185-187.*

MacVean, M.K., and S. Nicholls, 1988: A fine-resolution, two-dimensional numerical study of a cloud-capped boundary layer, *Proceedings of the 10th International Cloud Physics Conference, Bad-Hamburg, FRG, August 15-20, pp. 425-427.*

McKee, T.B. and S.K. Cox, 1974: Scattering of visible radiation by finite clouds, *J. Atmos. Sci., 31, 1885-1892.*

Rhys, Franz S., and A. Waldvogel, 1986: Fractal shape of hail clouds, *Phys. Rev. Lett., 56, 784-787.*

Schertzer, D., and S. Lovejoy, 1988: Multifractal simulations and analysis of clouds by multiplicative processes, *Atmos. Res., 21, 337-361.*

Stephens, G.L., 1976: The transfer of radiation through vertically non-uniform stratocumulus clouds, *Cont. Phys. Atmos., 49, 237-253.*

Stephens, G.L., 1985: Reply (to Harshvardan and Randall), *Mon. Wea. Rev., 113, 1834-1835.*

Welch, R.M. and B.A. Wielicki, 1985: A radiative parameterization of stratocumulus cloud fields, *J. Atmos. Sci., 42, 2888-2897.*